Comparative Study of PI, RST, Sliding Mode and Fuzzy Supervisory Controllers for DFIG based Wind Energy Conversion System

B. HAMANE[1, 2, ‡], M. L. DOUMBIA[1], M. BOUHAMIDA[2], A. DRAOU[3], H. CHAOUI[4] and M. BENGHANEM[2]

[1]Department of Electrical and Computer Engineering, Université du Québec à Trois-Rivières, QC, Canada

[2]Department of Electrical Engineering, University Mohamed Boudiaf, Oran, Algeria

[3]Department of Electrical Engineering,Islamic University of Madinah, Saudi Arabia

[4]Center for Energy Systems Research, Department of ECE, Tennessee Technological University, Cookeville, TN, USA

(bekhada.hamane@@univ-usto.dz; mamadou.doumbia@uqtr.ca; m_bouhamida@yahoo.com; adraou@yahoo.com; hchaoui@tntech.edu; mbenghanem69@yahoo.fr)

‡ Corresponding Author; B. HAMANE, e-mail: Bekhada.Hamane@uqtr.ca, Tel: +1 819 376 5011 ext. 3912,

Received: 15.10.2015 Accepted:30.11.2015

Abstract-This work aims to present a comparative study of four controllers for Double Fed Induction Generator (DFIG) based Wind Energy Conversion System (WECS). The DFIG is directly connected to the grid and driven by the rotor through an AC/DC/AC converter. A model was developed for each component (Turbine, DFIG and Rectifier-Filter-Inverter) of the wind system. The PWM control method is applied to the inverter to drive the DFIG from the rotor circuit. To ensure high performance and better enforcement of DFIG, a direct vector control strategy of active and reactive power of the stator has been developed. The synthesis of conventional PI controller and advanced RST, Sliding Mode (SM) and Fuzzy Supervisory (FS) controllers is performed. The system's performance has been tested and compared according to reference tracking, robustness, and disturbance rejection. A set of simulation studies are carried-out on a WECS model to prove the effectiveness of the proposed controllers design.

Keywords WECS, DFIG, RST Control, Sliding Mode Control, Fuzzy Supervisory Control.

1. Introduction

In recent years, the wind energy has become the fastest growing renewable energy source in the word. This is mainly due to the fact that it has received a thorough attention and has been considered as a way of fighting climate change. Control of the speed of the wind turbine is generally used to improve the energy production.

Wind Energy Conversion System (WECS) based on Double Fed Induction Generator (DFIG) provides various benefits. It reduces the stress on the mechanical structure and acoustical noise with the ability to control active and reactive power. A further advantage of DFIG system is that AC / DC / AC PWM converters connected between the grid and the rotor circuit of the induction generator are designed only for a part (approximately 30%) of the generator power [1]. In [2] PI control strategy has been investigated; the synthesis of this technique is purely algebraic and used the pole compensation based on a numerical method. [3-4] investigated a polynomial RST controller. This method is a sophisticated one and based on pole placement technique. Sliding Mode Control (SMC) controllers has been implemented in many areas because of its excellent properties, such as insensitivity to external perturbation and parameter variation [5].

New control strategies based on Fuzzy Supervisory (FS) have been proposed for the power control in the wind energy system [6]. In the FS based control, the qualitative process's expertise and experience of an operator or a field engineering should be embedded in the control strategy. However, FS control suffers from the absence of a formal development methodology, the difficulty of forecasting the stability and sturdiness of controlled systems [7].

In references [9], DFIG based wind power generation implementation has been presented, a Fuzzy PI gain scheduler for a vector controller is developed to control a DFIG used in a variable speed wind turbine. Reference [11] presents a theoretical analysis for wind turbine and DFIG is processed, given the mathematical models of system, a decoupling control of DFIG based on Fuzzy-PI controller is developed. Reference [12] proposes a grid connected wind power generation using a DFIG, which is driven by a direct AC/AC converter, that uses a stator flux vector control method and a space vector modulated matrix converter to control the stator power and the rotor current [12].

This paper presents a complete comparative analysis of proportional-Integral (PI), RST, SM and FS controllers for DFIG based WECS. Theoretical analysis, modeling and simulation studies are provided. Control strategies are developed for both the active and reactive powers in order to optimize the energy production of the WECS. The performance of the four control strategies is investigated and compared using reference tracking and robustness criteria.

To remedy the disadvantages of the PI controller, the synthesis of the other regulators namely, RST, SM and FS were proposed to improve the robustness of the direct control strategy to the parametric variations of the wind energy system based on a DFIG. The simulation results obtained show higher performance and better robustness of the three regulators as compared with those obtained by the PI controller. However, the performance of the Fuzzy Supervisory Controller is shown to be the best according to the set point criteria pursuit and robustness. The main contributions of this paper are the design and comparison of the various control laws (RST, Sliding Mode, and the Fuzzy Logic) for a wind energy system; and the development of control strategies that show their robustness through parametric variations.In view of the results obtained in this work, attractive prospects that can contribute to the improvement of the operating principle of the DFIG will be the subject of a future work. Figure 1 presents the Double Fed Induction Generator structure based in Wind Energy Conversion System.

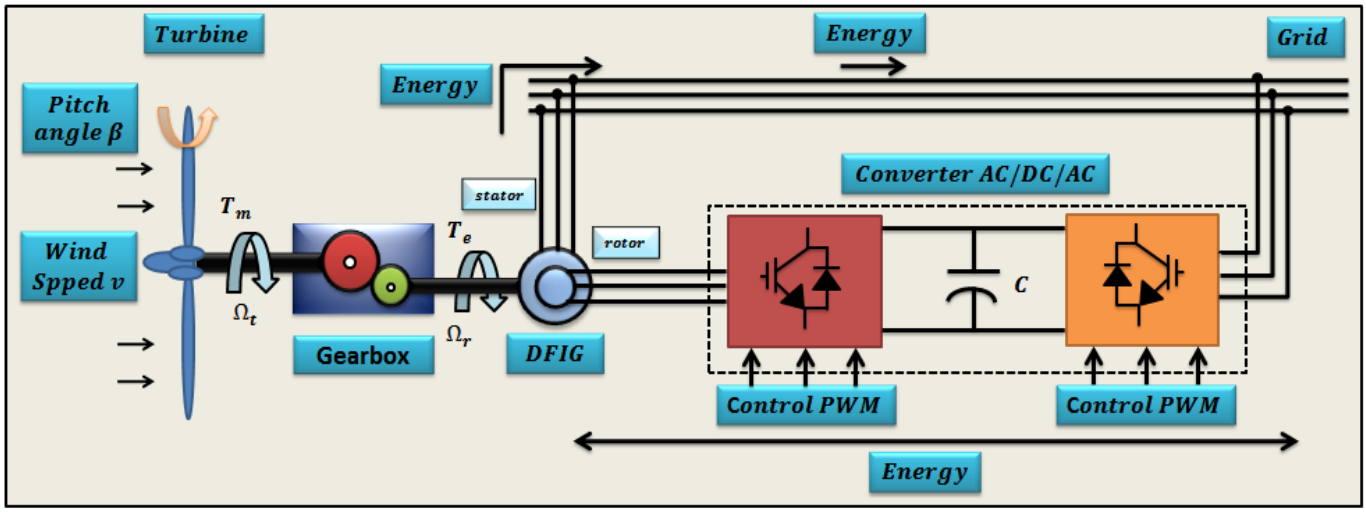

Fig. 1.DFIG based WECS structure.

2. Wind Energy Conversion System Modeling

2.1 Wind Turbine Model

As reported in [8, 22-23], the transferred mechanical power to the rotor is as given by:

$$P_t = \frac{1}{2}\pi\rho R^2 V^3 C_p(\lambda,\beta) \quad (1)$$

The input torque is then [8, 23-24]:

$$T_m = \frac{P_t}{\Omega_t} = \frac{\frac{1}{2}C_p(\lambda,\beta)\pi\rho R^2 V^3}{\Omega_t} \quad (2)$$

Where Ω_t, is the rotor's mechanical speed.

C_p is the power coefficient which depends on the pitch angle β and the tip speed ratio λ [9].

$$C_p(\lambda,\beta) = c_1\left(\frac{c_2}{\lambda_i} - c_3\beta - c_4\right)e^{\frac{-c_5}{\lambda_i}} + c_6\lambda \quad (3)$$

With: $c_1 = 0.5176,\ c_2 = 116, c_3 = 0.4, c_4 = 5, c_5 = 21,$ $c_6 = 0.0068$

Where $\lambda_i$is given by [23-24]:

$$\frac{1}{\lambda_i} = \left(\frac{1}{\lambda+0.08\beta} - \frac{0.035}{\beta^3+1}\right) \quad (4)$$

And the tip speed ratio λ is found [10, 23-24] as:

$$\lambda = \frac{\Omega_t.R}{v} = \frac{\Omega_{mec}.\varepsilon.R}{v} \quad (5)$$

The block diagram given in Figure 2 represents the dynamic model of the turbine.

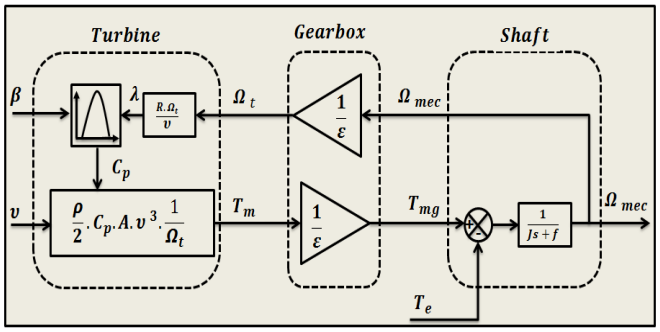

Fig. 2. Block diagram of the dynamic model of the turbine.

2.2 Double Fed Induction Generator Model

In rotating field reference frame, the Park's transformation and two-phase reference model of the wound rotor induction machine [25-26] are illustrated in Figure 3:

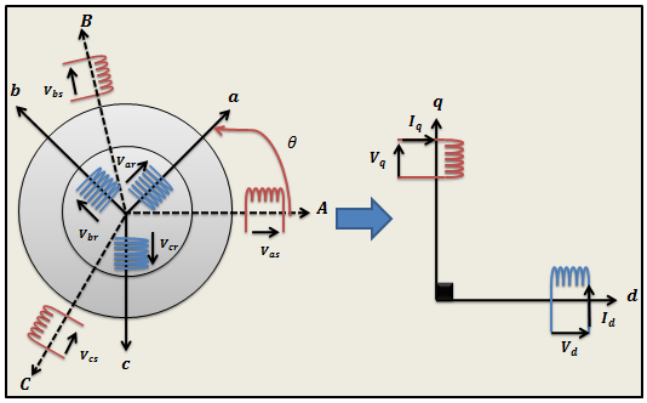

Fig. 3. Park's transformation and two reference model of the DFIG.

Electromagnetic and mechanical torques equations are [12, 23, 26]:

$$\begin{cases} T_e = -\frac{3}{2}P\frac{L_m}{L_s}(\varphi_{ds}I_{dr} - \varphi_{qs}I_{ds}) \\ J\frac{d\Omega_{mec}}{dt} + f\Omega_{mec} = T_e - T_{mg} \end{cases} \quad (6)$$

The stator and rotor voltages are represented by the following equations [12, 23]:

$$\begin{cases} V_{ds} = R_s I_{ds} + \frac{d\varphi_{ds}}{dt} - \omega_s\varphi_{qs} \\ V_{qs} = R_s I_{qs} + \frac{d\varphi_{qs}}{dt} - \omega_s\varphi_{ds} \\ V_{dr} = R_r I_{dr} + \frac{d\varphi_{dr}}{dt} - (\omega_s - \omega_{mec})\varphi_{qr} \\ V_{qr} = R_r I_{qr} + \frac{d\varphi_{qr}}{dt} + (\omega_s - \omega_{mec})\varphi_{dr} \end{cases} \quad (7)$$

$$\begin{cases} \varphi_{ds} = L_s I_{ds} + L_m I_{dr} \\ \varphi_{qs} = L_s I_{qs} + L_m I_{qr} \\ \varphi_{dr} = L_r I_{dr} + L_m I_{ds} \\ \varphi_{qr} = L_r I_{qr} + L_m I_{qs} \end{cases} \quad (8)$$

2.3 Modeling of the Power Electronic Converters

2.3.1 Modeling of three phase diode rectifier

The rectifier is an AC to DC converter and its input voltage is defined as follow [13]:

$$\begin{cases} V_{sa}(t) = V_{rms}\sqrt{2}\sin(2\pi f_s t) \\ V_{sb}(t) = V_{rms}\sqrt{2}\sin\left(2\pi f_s t - \frac{2\pi}{3}\right) \\ V_{sc}(t) = V_{rms}\sqrt{2}\sin\left(2\pi f_s t - \frac{4\pi}{3}\right) \end{cases} \quad (9)$$

Then, the output voltage of the rectifier is [13]:

$$V_{rec}(t) = \mathrm{Max}[V_{sa}(t).V_{sb}(t).V_{sc}(t)] - \mathrm{Min}[V_{sa}(t).V_{sb}(t).V_{sc}(t)] \quad (10)$$

2.3.2 Modeling of the filter

Low pass (LC) filter (Figure 4) is used to remove the high frequency components [13]. The filter design is determined by the system of equations [13]:

$$\begin{cases} \frac{dI_d}{dt} = \frac{V_{rec} - V_{dc}}{L_f} \\ \frac{dV_{dc}}{dt} = \frac{I_d - I_s}{C_f} \end{cases} \quad (11)$$

The filter's transfer function is presented by:

$$F(p) = \frac{V_{dc}(p)}{V_{rec}(p)} = \frac{1}{L_f C_f p + 1} \quad (12)$$

This transfer function is of the first order whose cut off frequency is:

$$f_c = \frac{1}{2\pi\sqrt{L_f C_f}} \quad (13)$$

To eliminate the second and higher harmonics, the following condition is required: $f_c = 2.f_{rec}$, withf_{rec} is the frequency of the rectified voltage V_{rec}.

2.3.3 Modeling of the inverter

The design of the inverter is determined by the system of equations [13]:

$$\begin{bmatrix} V_{ra} \\ V_{rb} \\ V_{rc} \end{bmatrix} = \frac{V_{dc}}{3}\begin{bmatrix} 2 & -1 & -1 \\ -1 & 2 & -1 \\ -1 & -1 & 2 \end{bmatrix}\begin{bmatrix} S_a \\ S_b \\ S_c \end{bmatrix} \quad (14)$$

V_{ra} , V_{rb} and $V_{rc}$are the output voltages of the inverter; S_a , S_b and S_c are control signals of the inverter.

Figure 4 shows the three-phase variable frequency converter [25].

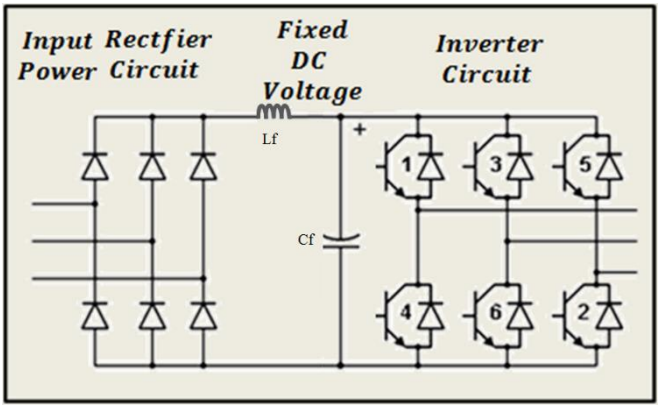

Fig. 4. Three phase variable frequency inverter.

3. DFIG Control of Active and Reactive Power

To achieve the vector control of the active and reactive power of the stator as indicated in Figure 5a, $d-q$ reference frame which is synchronized to the stator flux has been selected [5, 14, 19, 22]. The stator flux vector is aligned with the axis d, so $\varphi_{ds} = \varphi_s$and $\varphi_{qs} = 0$ and the equation of electromagnetic torque becomes [22]:

$$T_e = -\frac{3}{2}P\frac{L_m}{L_s}(\varphi_{ds}I_{dr}) \quad (15)$$

Hence, the active power and the electromagnetic torque only depend on the q-axis component of the rotor current. This torque can be analysed as a disturbance for the wind turbine and considered with a negative value. For medium and high power machines, the stator resistance R_s can be neglected [12], and the stator fluxes and voltages are expressed as below [5, 22]:

$$\begin{cases} \varphi_{ds} = \varphi_s = L_s I_{ds} + L_m I_{dr} \\ \varphi_{qs} = 0 = L_s I_{qs} + L_m I_{qr} \end{cases} \quad (16)$$

$$\begin{cases} V_{ds} = 0 \\ V_{qs} = V_s = \omega_s\varphi_{ds} \end{cases} \quad (17)$$

Figure 5 represents the direct active and reactive power control scheme of DFIG driven by a conventional converter AC/DC/AC [25-26]:

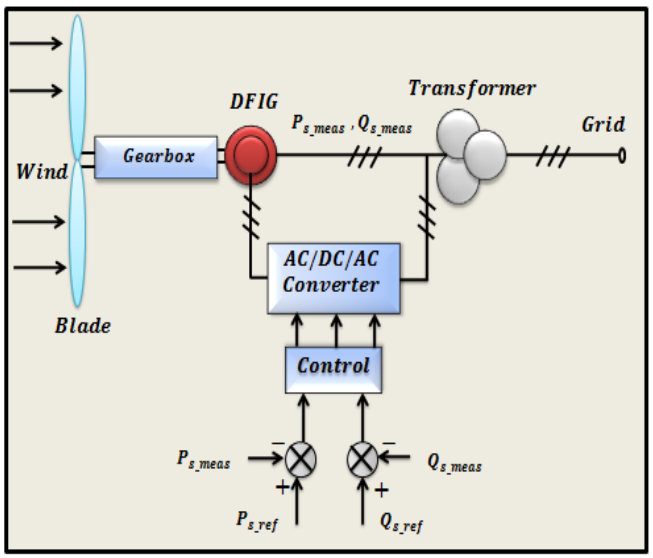

Fig. 5. Direct power control between the stator and the grid.

The stator's powers and rotor's voltages are presented as [5]:

$$\begin{cases} P_s = -V_s \frac{L_m}{L_s} I_{qr} \\ Q_s = -V_s \frac{L_m}{L_s} I_{dr} + V_s \frac{\varphi_s}{L_s} \end{cases} \quad (18)$$

$$\begin{cases} V_{dr} = R_r I_{dr} + L_r \sigma \frac{d}{dt} I_{dr} - g\omega_s L_r \sigma I_{qr} \\ V_{qr} = R_r I_{qr} + L_r \sigma \frac{d}{dt} I_{qr} + g\omega_s L_r \sigma I_{dr} + g \frac{L_m V_s}{L_s} \end{cases} \quad (19)$$

$$\sigma = \left(1 - \frac{L_m^2}{L_s L_r}\right) \quad (20)$$

In steady state, the derivative terms $\left(\frac{d}{dt} I_{dr}\right.$ and $\left.\frac{d}{dt} I_{qr}\right)$ in (19) could be neglected [5, 22]. The block-diagram of the system is presented in Figure 6. Knowing (18) and (19), it is then possible to synthesize the regulators.

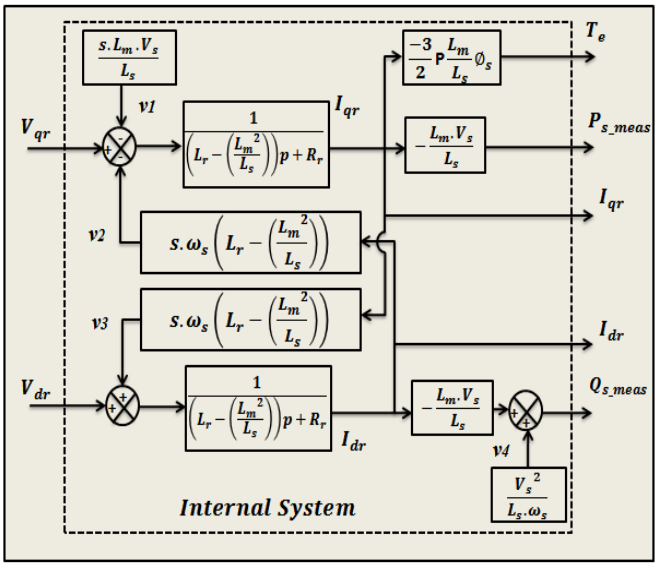

Fig. 6. Control scheme of the system.

Where, ω_s is the grid angular speed, ω_{mec} is rotor speed and s is the slip respectively. The slip is defined by the ratio between the speed the mechanical angular and that of the rotor $\left(s = \frac{\omega_s - \omega_{mec}}{\omega_s}\right)$.

4. Controllers Design

PI, RST, SM and FS controllers are designed to achieve active and reactive reference power tracking; robustness to parameter variations and disturbance rejection.

4.1 Design of the PI Controller

Figure 7 shows the block diagram scheme of the power control loop [5].

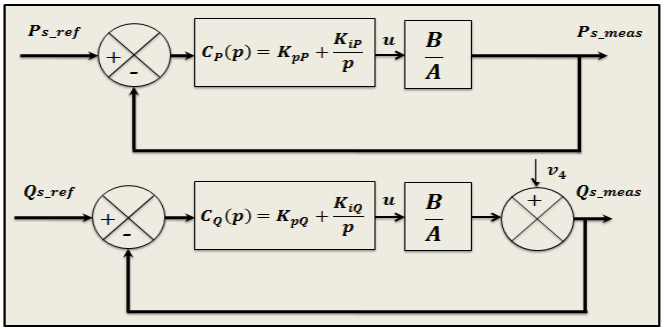

Fig. 7. Equivalent PI control scheme.

The controllers' gains are chosen symmetric to preserve the symmetrical property of the open loop circuit [5].

$$\begin{cases} K_{pP} = K_{pQ} = K_p \\ K_{iP} = K_{iQ} = K_i \end{cases} \quad (21)$$

And the terms of A and B are [5]:

$$\begin{cases} A = R_r + pL_r\left(1 - \frac{L_m^2}{L_s L_r}\right) \\ B = \frac{L_m V_s}{L_s} \end{cases} \quad (22)$$

The open loop transfer function of these regulators is [5]:

$$G(p) = \left(\frac{p + \frac{K_i}{K_p}}{\frac{p}{K_p}}\right).\left(\frac{\frac{L_m.V_s}{L_r.L_s.\sigma}}{p + \frac{L_s.R_r}{L_r.L_s.\sigma}}\right) \quad (23)$$

To eliminate the zero of the transfer function [24], a compensation method is used [5, 24]. As such:

$$\frac{K_i}{K_p} = \frac{R_r}{L_r \sigma} \quad (24)$$

The open loop transfer function becomes:

$$G(p) = \frac{K_p \frac{L_m.V_s}{L_r.L_s.\sigma}}{p} \quad (25)$$

The closed loop transfer function response time and the controller gains are expressed by:

$$H(p) = \frac{1}{1 + p\tau_r} \quad (26)$$

$$\tau_r = \frac{1}{K_p} \frac{L_r.L_s.\sigma}{L_m.V_s} \quad (27)$$

$$\begin{cases} K_p = \frac{L_r.L_s.\sigma}{\tau_r.L_m.V_s} \\ K_i = \frac{L_s.R_r}{\tau_r.L_m.V_s} \end{cases} \quad (28)$$

4.2 Design of the RST Controller

In this section, the RST power controller is designed as two degrees of freedom system. The main advantage of such a control system is the possibility for the designer to specify independently the system's performance from the reference variation (trajectory tracking). RST acronym comes from the

name of three polynomials to be determined in order to achieve effective control. The method uses pole placement technique using an arbitrary stability polynomial D(p). Then the parameters S(p) and R(p) are calculated according to the Bezout equation [4, 19]:

$$D = AS + BR \tag{29}$$

With: $\deg(D(p)) = \deg(A(p)) + \deg(S(p))$

The closed loop system of the RST controller is represented by the block diagram scheme [13, 19] as shown in Figure 8:

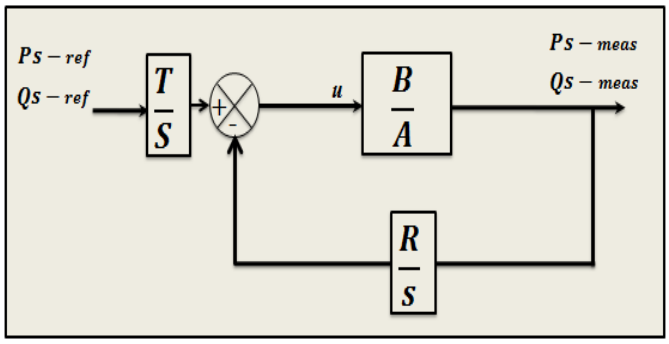

Fig. 8. RST controller structure.

Polynomials of the proposed model are expressed as:

$$\begin{cases} A(p) = a_1 p + a_0 \\ B(p) = b_0 \\ D(p) = d_3 p^3 + d_2 p^2 + d_1 p + d_0 \\ R(p) = r_1 p + r_0 \\ S(p) = s_2 p^2 + s_1 p + d_0 \end{cases} \tag{30}$$

The polynomial $D(p) = C(p)F(p)$ can be obtained from the pole placement technique and is shown as:

$$D = \left(p + \frac{1}{T_c}\right)\left(p + \frac{1}{T_f}\right)^2 \tag{31}$$

$P_C = -1/T_C$ is the pole of polynomial C and $P_f = -1/T_f$ is the double pole of the polynomial filter F.

$$\begin{cases} P_c = 5P_a = -5\frac{L_s R_r}{(L_r L_s - L_m^2)} \\ T_c = \frac{1}{P_c} \\ T_f = \frac{1}{3}T_c \end{cases} \tag{32}$$

The following conditions are applied to accelerate the system:

$$D(p) = (p - 5P_a)(p - 15P_a)^2 \tag{33}$$

By identifying equations (30) and (33), the polynomial's coefficients are determined and equated to R(p) and S(p) by the well-known Sylvester's matrix [4, 19]. Hence, we may deduce the RST controller's parameters readily as:

$$\begin{cases} d_3 = a_1 s_2 \rightarrow s_2 = \frac{d_3}{a_1} \\ d_2 = a_1 s_1 \rightarrow s_1 = \frac{d_2}{a_1} \\ d_1 = a_0 s_1 + b_0 r_1 \rightarrow r_1 = \frac{d_1 - a_0 s_1}{b_0} \\ d_1 = b_0 r_0 \rightarrow r_0 = \frac{d_0}{b_0} = T \end{cases} \tag{34}$$

4.3 Design of the Sliding Mode Controller

The Sliding Mode controller has had great success over the last few years because of the simplicity of its implementation [24] and its strength against the uncertain systems and from external disturbances. Sliding mode control brings back the state trajectory to the sliding surface [2, 10-11, 19, 24]. This trajectory determination consists of three parts: choice of the sliding surface [24], the convergence condition and computation of the control [24]. It can be applied to active and reactive powers which can be expressed as the derivative of sliding surface γ.

$$\begin{cases} \dot{\gamma}(P) = \left(\dot{P}_{s-ref} - \dot{P}_{s-mes}\right) \\ \dot{\gamma}(Q) = \left(\dot{Q}_{s-ref} - \dot{Q}_{s-mes}\right) \end{cases} \tag{35}$$

From equation (18), the derivative expressions of active and reactive power are:

$$\begin{cases} \dot{\gamma}(P) = \left(\dot{P}_{s-ref} - V_s \frac{L_m}{L_s} \dot{I}_{rq}\right) \\ \dot{\gamma}(Q) = \left(\dot{Q}_{s-ref} - V_s \frac{L_m}{L_s} \dot{I}_{rd}\right) \end{cases} \tag{36}$$

$$\begin{cases} \dot{\gamma}(P) = \left(\dot{P}_{s-ref} - V_s \frac{L_m}{L_s L_r \sigma}\left(V_{rq} - R_r I_{rq}\right)\right) \\ \dot{\gamma}(Q) = \left(\dot{Q}_{s-ref} - V_s \frac{L_m}{L_s L_r \sigma}\left(V_{rd} - R_r I_{rd}\right)\right) \end{cases} \tag{37}$$

During the sliding mode and steady state:

$$\begin{cases} \gamma(P) = 0; \quad \gamma(Q) = 0 \\ \dot{\gamma}(P) = 0; \quad \dot{\gamma}(Q) = 0 \\ V_{rq}^n = 0 \; ; \quad V_{rd}^n = 0 \end{cases} \tag{38}$$

Replacing V_{qr} by $V_{qr}^{eq} + V_{qr}^n$, and V_{dr} by $V_{dr}^{eq} + V_{dr}^n$, equation (37) becomes:

$$\begin{cases} \dot{\gamma}(P) = \left(\dot{P}_{s-ref} - V_s \frac{L_m}{L_s L_r \sigma}\left(V_{rq}^{eq} + V_{rq}^n - R_r I_{rq}\right)\right) \\ \dot{\gamma}(Q) = \left(\dot{Q}_{s-ref} - V_s \frac{L_m}{L_s L_r \sigma}\left(V_{rd}^{eq} + V_{rd}^n - R_r I_{rd}\right)\right) \end{cases} \tag{39}$$

Then the equivalent command V_{qr}^{eq} and V_{dr}^{eq} can be written as:

$$\begin{cases} V_{rq}^{eq} = \left(-\dot{P}_{s-ref} \frac{L_s L_r \sigma}{L_m V_s} + R_r I_{rq}\right) \\ V_{rd}^{eq} = \left(-\dot{Q}_{s-ref} \frac{L_s L_r \sigma}{L_m V_s} + R_r I_{rd}\right) \end{cases} \tag{40}$$

During the convergence mode, the condition for power; $\gamma(P)\dot{\gamma}(P) \leq 0, \gamma(Q)\dot{\gamma}(Q) \leq 0$ is verified, so:

$$\begin{cases} \dot{\gamma}(P) = \left(-V_s \frac{L_m}{L_s L_r \sigma} V_{rq}^n\right) \\ \dot{\gamma}(Q) = \left(-V_s \frac{L_m}{L_s L_r \sigma} V_{rd}^n\right) \end{cases} \tag{41}$$

Therefore, the switching term is given by:

$$\begin{cases} V_{rq}^n = K_1 \text{sign}\left(\gamma(P)\right) \\ V_{rd}^n = K_2 \text{sign}\left(\gamma(Q)\right) \end{cases} \tag{42}$$

To verify the condition of stability of the system, parameters K_1 and K_2 must be positive. To alleviate the overshoot of the reference voltage V_{qr} and V_{dr}, it is often useful to add a voltage limiter. Figure 9 and 10 show SM control structure for active and reactive power:

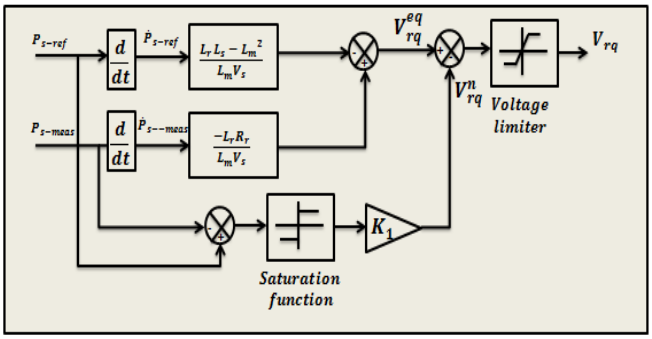

Fig. 9. Sliding mode controller structure for active power control.

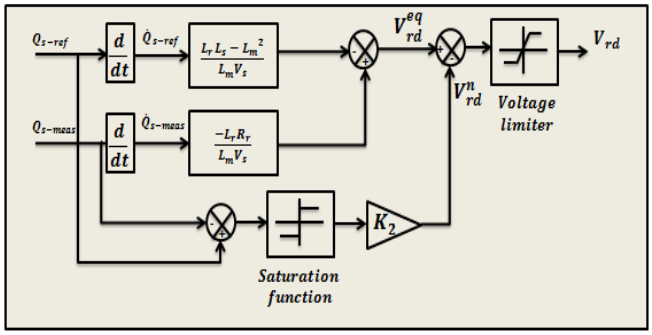

Fig. 10. Sliding mode controller structure for reactive power control.

4.4 Design of the Fuzzy supervisory controller

From the operational characteristics and control requirements of Doubly Fed Induction Generator, a control technique based on Fuzzy Supervisory is developed [9, 18, 20-21]. The Gain Scheduling method is used for the adaptation of the PI control gains as shown in Figure 11. Figure 12 shows the schematic diagram of the PI with FS controller.

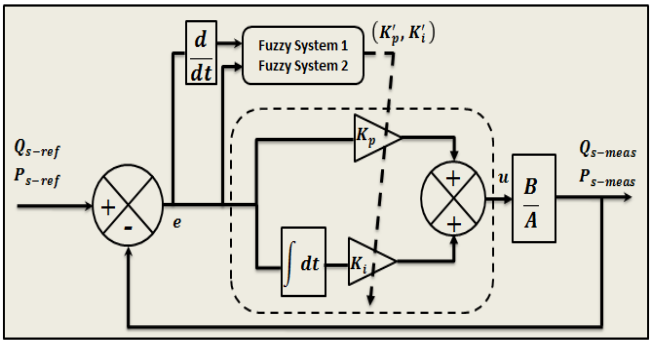

Fig. 11. Structure of Fuzzy Supervisory Control.

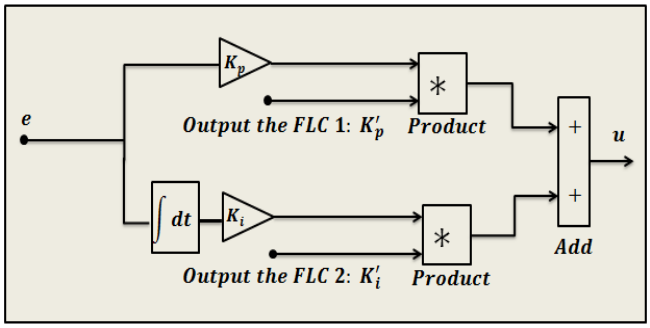

Fig. 12. Structure of PI with FS Controller.

The controller will tune the parameters (K_p, K_i) of the conventional PI in order to obtain new parameters based on the error and its derivative and may span all operating conditions [16, 18]. Thus, they are normalized in the interval $K_p \in [0-5]; K_i \in [0-0{,}6]$ utilizing the following linear transforms [15, 21]:

$$\begin{cases} K_p = (K_{pmax} - K_{pmin})K'_p + K_{pmin} \\ K_i = (K_{imax} - K_{imin})K'_i + K_{pmin} \end{cases} \quad (43)$$

After the K'_p and K'_i values have been obtained, the new parameters of the PI regulator are calculated by the equation [12]-[17]:

$$\begin{cases} K'_p = (K_p - K_{pmin})/(K_{pmax} - K_{pmin}) \\ K'_i = (K_i - K_{imin})/(K_{imax} - K_{imin}) \end{cases} \quad (44)$$

Where e and de/dt represent the error and its derivative, respectively and are considered as the input of the controller whereas the output signals are the normalized values of the proportional and integral actions, K'_p, K'_i, respectively. Input signals comprise three membership functions while the gains K'_p and K'_i have four and two functions, respectively.

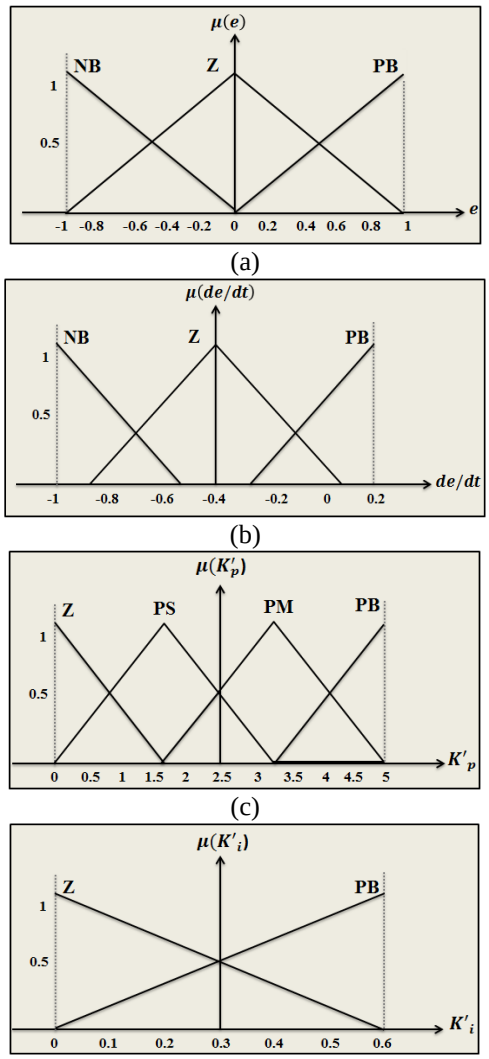

Fig.13. Membership functions: (a) error, (b) derivative error, (c) K'_p gain, (d) K'_igain

Figure 13 (a) and (b) show the input signal represented by the membership functions of both power controllers. Whereas Fig. 13 (c) and (d) show the membership functions for the both the proportional and integral gains of the power controllers.
Center of gravity approach [17] is used to defuzzify the output variable of the system:

$$u = \frac{\sum_{i=1}^{m} \mu(x_i).x_i}{\sum_{i=1}^{m} \mu(x_i)} \quad (45)$$

Table 1 and 2 show the power controller's fuzzy rules.

Table 1. The basis of fuzzy control rules for K'_p

U		e		
		NB	Z	PB
de	NB	Z	Z	Z
	Z	PB	PS	PB
	PB	Z	PM	Z

Table 2. The basis of fuzzy control rules forK'_i

U		e		
		NB	Z	PB
de	NB	PB	PB	PB
	Z	Z	PB	Z
	PB	PB	PB	PB

5. Results

In order to study and compare efficiently the proposed controllers, a series of simulation tests have been carried out in Matlab/Simulink environment using SPS toolbox. The PWM inverter on the rotor side of the DFIG (P_m = 1.5 MW) is controlled. The controllers' performances are analysed and compared using two different specifications, i.e. the tracking of the references representing the robustness and the tracking based on changes of the system's parameters. WECS system's parameters are listed in Appendix in Tables 3 and 4.

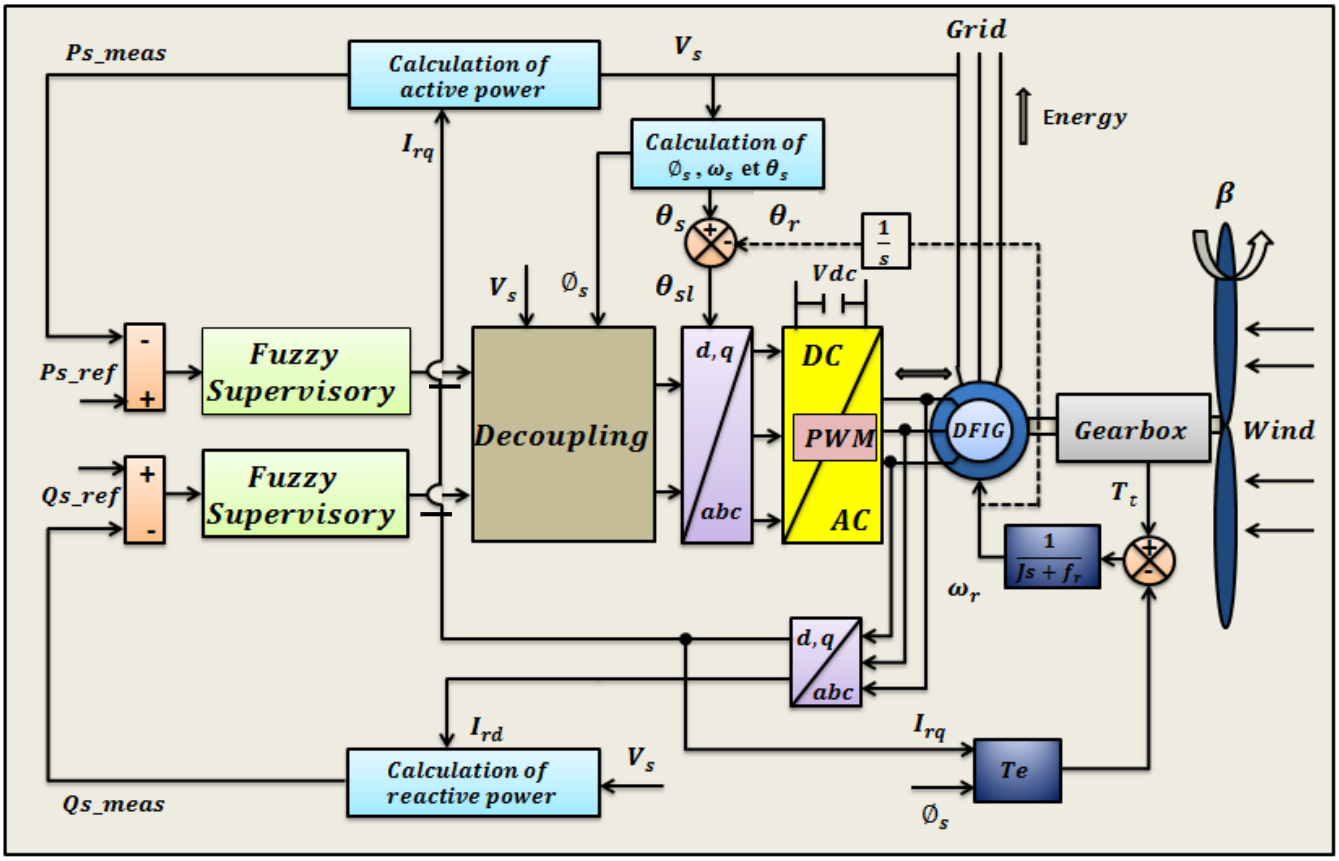

Fig. 14. Controller Direct control loop of DFIG using Fuzzy Supervisory control.

5.1 Converters input and output voltages

Figure 15 presents simulation results of the rectifier and the filter, where $V_a(t), V_b(t)$ and $V_c(t)$ are respectively the input voltages of the grid. $V_{rec}(t)$ is the output voltage of the rectifier and $V_{dc}(t)$ is output voltage of the low-pass (LC) filter. The control signal and output voltage of the inverter controlled by Pulse Width Modulation (PWM) are respectively presented in Figure 16 and 17.

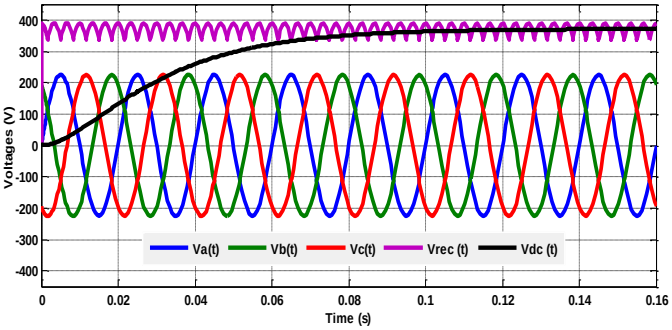

Fig. 15. Input and output voltages of the rectifier and filter.

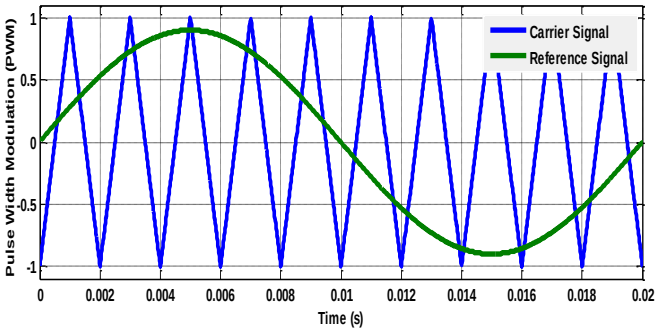

Fig. 16. Carrier signal and reference signal of PWM.

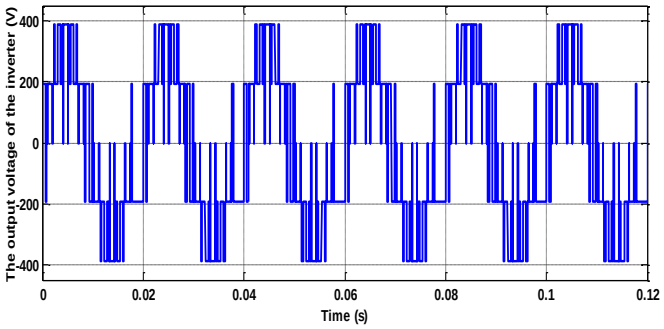

Fig. 17. The output voltage of the inverter.

5.2 *Control of power factor*

During the first test, the stator reactive power is set zero to ensure unity power factor at the stator side in order to optimize the quality of the energy returned to the grid. The active power follows the reference value and the set of active power helps to keep the power factor of wind turbine to its optimal value as shown inFigure 18. In the second test,reactive powerof− 0.6MVAr was generated while the activepoweris fixed to− 1.2MW, asshown inthe Fig 19.

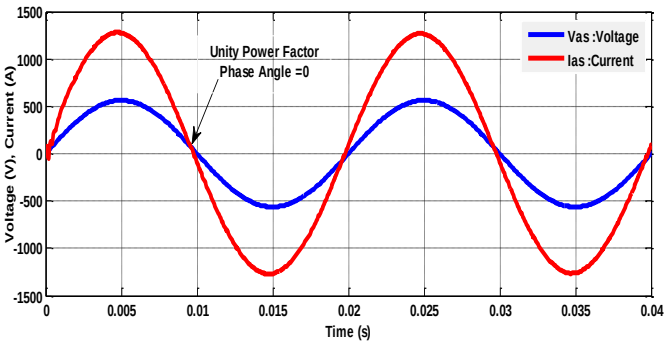

Fig. 18. Unity power factor control.

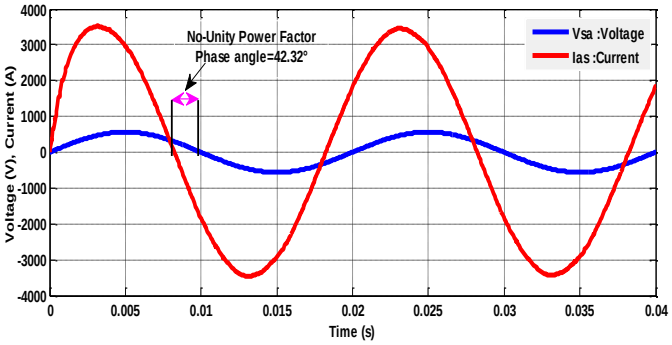

Fig. 19. No-unity power factor control.

In Figure 18, the control of the active power factor is made to be exactly a unity ($\cos\emptyset = 1$), so a zero phase shift is maintained. In Fig 19, thepowerfactoris 0.73 which corresponds to a phase difference of$\emptyset = 42.32°$.

5.3 *Influence of reactive power on the rotor current*

To see the impact of reactive power on the magnitude and the phase of the rotor current waveform, the control system regulates not onlypower, but also the power factor that allows the DFIG to operate with optimal performance.

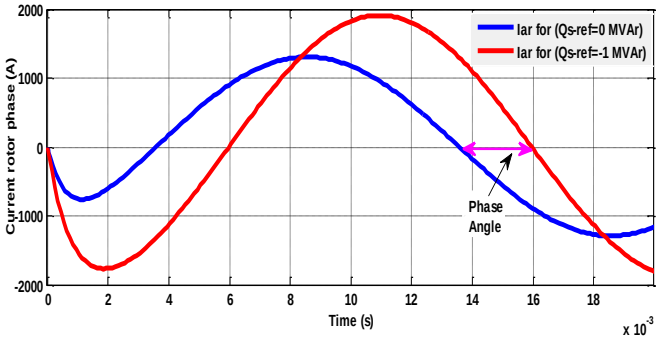

Fig. 20. Controlling the phase angle of the rotor current.

The decoupling of the frequencies of the inverter and the grid allows choosing independently the phase of the rotor currents. Fig 20 shows the impact of reactive power change on the amplitude and phase of the currents of the rotor.

5.4 *Reference tracking*

Initially, the machine is driven without load at $N_s = 1500$ rpm. Then, different step values of input power are implemented. Dynamic responses of controllers: PI, RST, SM, FS are illustrated in Fig 21. Through the comparative study, it can be seen that the various regulators, i.e., PI, RST, SM and FS, give almost the same profile for the different tests applied to the DFIG, but with better transient response time in the case of the FS.

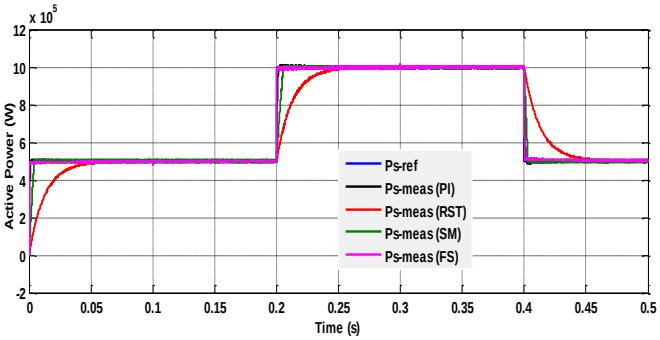

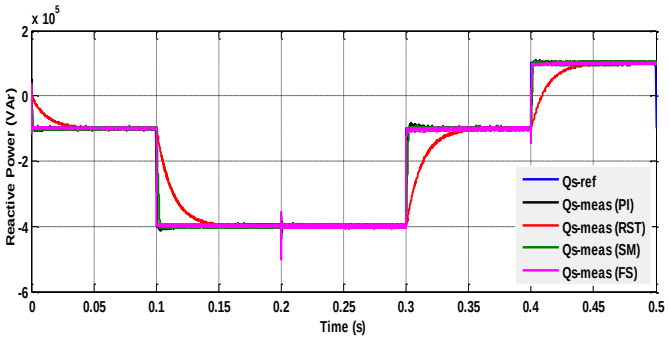

Fig. 21. Dynamic responses of PI, RST, SM and FS controllers for a step change of active and reactive power.

The step references are correctly followed and there is no error on the powers in steady state. The uncoupling between the two active and reactive powers is ideally noted. Negative sign of the reactive power shows that the machine operates in generator mode; for the driving mode, reactive power automatically turns positive.

5.5 Robustness

In order to investigate the robustness of the controllers, the nominal value of $R_r$is doubled, the values of $L_s$and $L_r$are increased by 10% of their rated values, and the value of L_m being reduced to 90% of its nominal value.

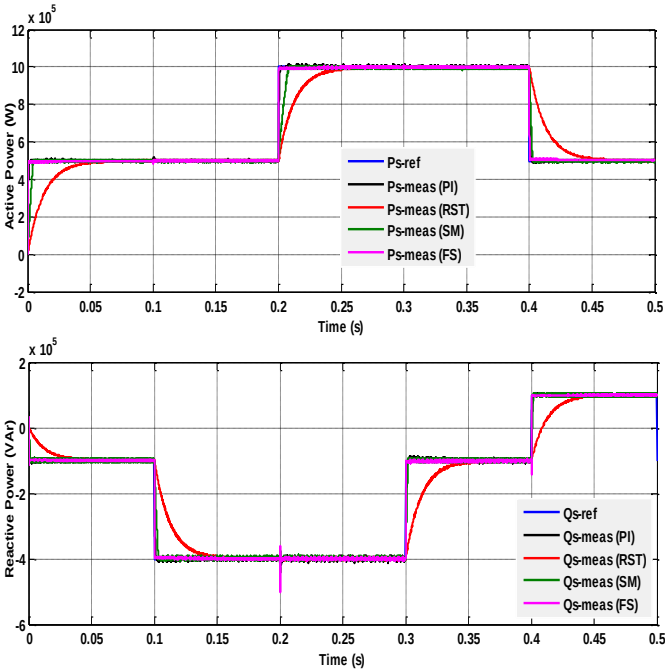

Fig. 22. Active and reactive power behavior using PI, RST, SM and FS controllers with 50% variation of R_r.

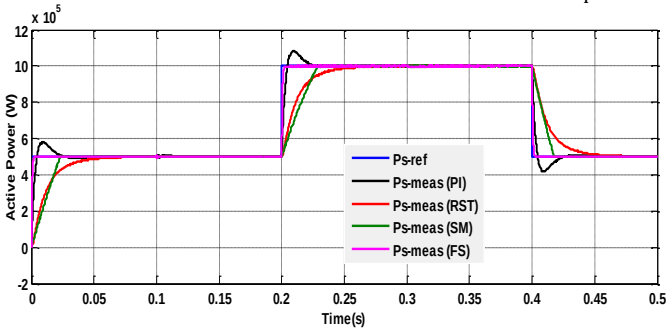

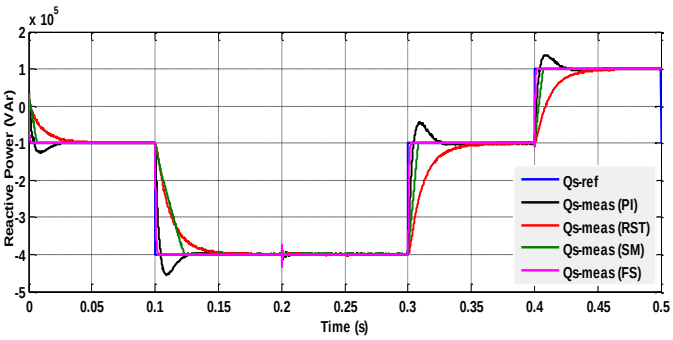

Fig. 23. Active and reactive power behavior using PI, RST, SM and FS controllers with +10% variation of L_s.

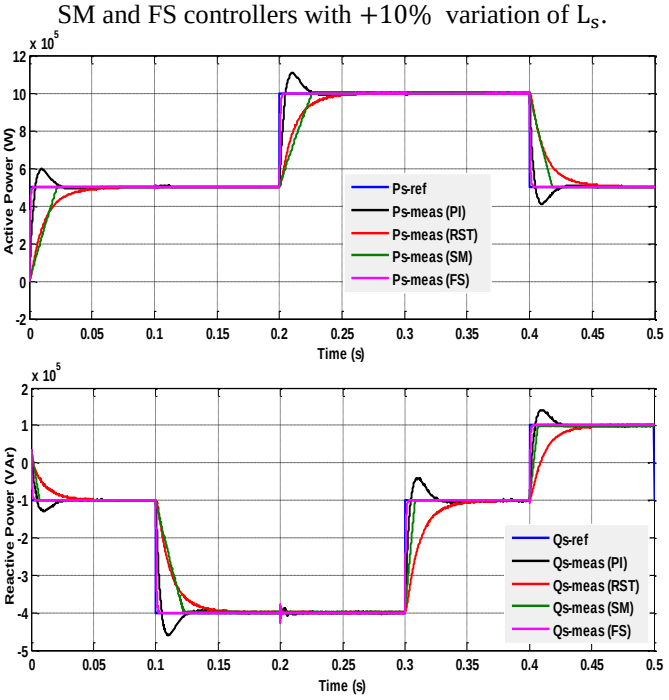

Fig. 24. Active and reactive power behavior using PI, RST, SM and FS controllers with +10% variation of L_r.

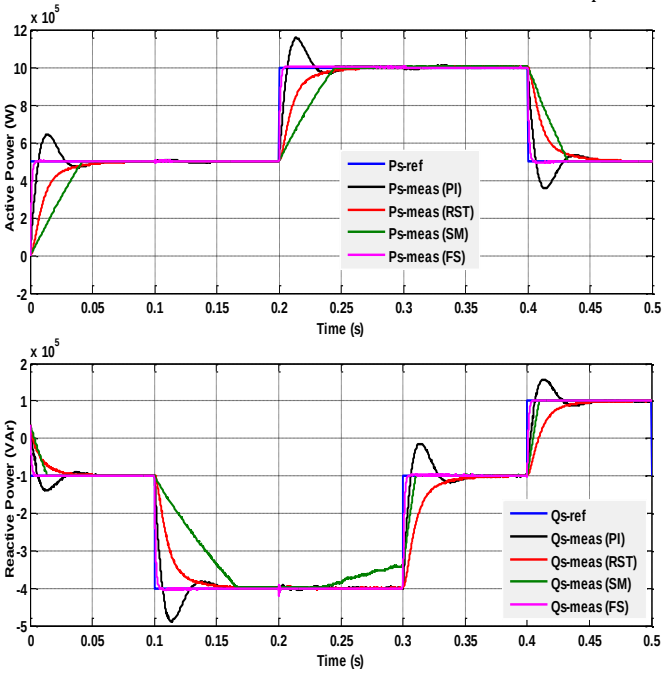

Fig. 25. Active and reactive power behavior using PI, RST, SM and FS controllers with −10% variation of L_m.

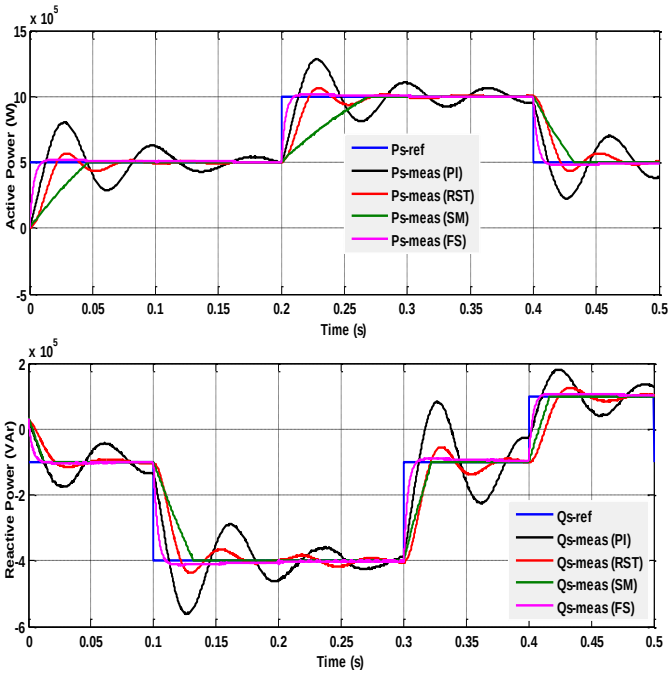

Fig. 26. Active and reactive power behavior using PI, RST, SM and FS controllers with simultaneously variation of parameters.

Through the comparative study, the objective of robustness tests is to compare the performance of the controllers when machine's parameters change. The impact of resistance and inductance variations on active and reactive power is investigated (Figures 22, 23, 24, 25).Figure 26 shows simulation results when several parameters (R_r+50 %, L_s+20 %, L_r+20 % and L_m-20 %) change at the same time. Simulation results show that the variation of several parameters at the same time deteriorates the performance of the FS controller in terms of response time, but not in terms of tracking unlike the PI controllers, which are degraded completely with these variations.

5.6 Comparison of the behavior of the four controllers

For step changes of active and reactive powers, the FS controller achieves the best transient response (Fig 27).

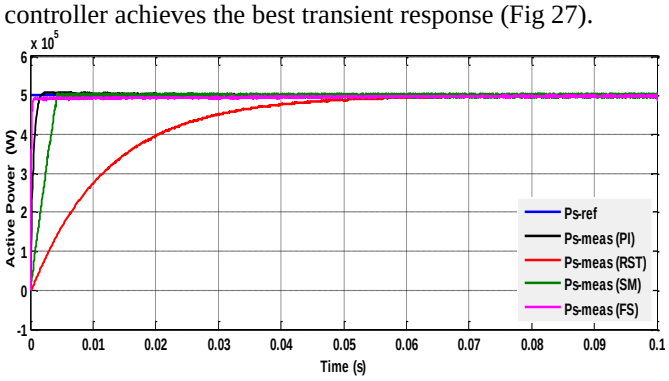

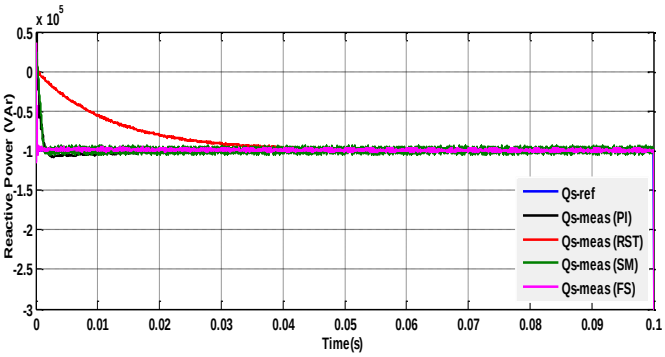

Fig. 27. Comparative response of the active and reactive power control using PI, RST, SM and FS controllers.

The results show that, with the FS controller, the response time is significantly reduced, a small overshoot and oscillations are damped more quickly compared to the other controllers. The transient state of the system with FS controller is better than the other controllers.

6. Conclusion

This article introduced a wind energy conversion system based on the wound rotor induction generator connected to grid. The direct vector control of stator's active and reactive power was performed using Matlab/Simulink. The investigated results show that the mathematical modeling based on the knowledge of voltages and the currents can be used to control the powers. Furthermore, the power factor could be controlled by a PI controller. The comparative study of the active and reactive power control revels that the PI, RST, SM and FS controllers performed quite well under ideal conditions when there are no perturbation and no parameters variations. However, in the case of parameters variations (i.e., change in rotor's resistance and mutual inductance), the Fuzzy Supervisory Controller seems more robust that all others controllers. The main contributions of this proposed work can be summarized as follows: design and comparison of the various control laws (RST, Sliding Mode, and the Fuzzy Logic) for a wind energy system and the development of control strategies that show their robustness through parametric variations.

References

[1] Belmokhtar, K., Doumbia, M. L., Agbossou, K., "Modelling and fuzzy logic control of DFIG based wind energy conversion systems", IEEE, International Symposium on Industrial Electronics (ISIE), Hangzhou, China, 2012.

[2] Soltani, J., Payam, A. F., "A robust adaptive sliding-mode controller for slip power recovery induction machine drives," Power Electronics and Motion Control Conference, vol.3, pp. 1-6, 2006.

[3] Bouhamida, M., Denai, M.A., "Robust stabilizer of electric power generator using H∞ with placement constraints", Journal of Elec. Eng. (JEE), Vol. 56, No. 7-8, pp. 176-182, 2005.

[4] Hachicha, F., Krichen, L., "Performance analysis of a wind energy conversion system based on a doubly-fed induction generator", IEEE, 8th International Multi

Conference on Systems, Signals & Devices, pp.978-984, 2011.
[5] Poitiers, F., Machmoum, M., Le Doeuff, R. and Zaim, M.E., "Control of a doubly-fed induction generator for wind energy conversion systems," IEEE Trans, Renewable Energy, Vol. 3, N°. 3, pp.373-378, 2001.
[6] Gilbert, C., Sousa, D., Bose, B. K., "Fuzzy logic applications to power electronics and drives - an overview," IEEE, International Conference on Industrial Electronics, Control, and Instrumentation, Vol. 1, Orlando, FL, pp.57-62, 1995.
[7] Slootweg, J. G., Polinder, H., Kling, W. L., "Initialization of wind turbine models in power systems dynamic simulations," IEEE, Power Tech Conference, Porto Portugal, Vol. 4, 2001.
[8] Siegfried Heier, Grid integration of wind energy conversion systems, John Wiley & Sons Ltd, ISBN 0-471-97143-X, 1998.
[9] Soloumah, H. M., Kar, N. C., "Fuzzy logic based vector control of a doubly-fed induction generator for wind power application," Wind Engineering, vol. 30, no. 3, pp. 201-223. April 2006.
[10] Islam, M.R., Youguang, G., Jian, G.Z., "Steady state characteristic simulation of DFIG for wind power system," IEEE, Electrical and Computer Engineering (ICECE), pp. 151-154, Dhaka 2010.
[11] Slotine, J.J., "Adaptive Sliding controller synthesis for nonlinear systems", International Journal of Control, Vol 43. N°6, pp 1631-1651, 1986.
[12] Zhang, L., Watthansarn, C., Shehered, W., "A matrix converter excited doubly-fed induction machine as a wind power generator," IEEE, Seventh International Conference on Power Electronics and Variable Speed Drives, vol. 2, pp. 532-537, 1998.
[13] Messaouda, M., Ouddane, A, Contrôle des puissances actives et réactives de la MADA intégrée dans un système éolien, Master thesis, University Mohamed Boudiaf USTO, Algeria, 2011.
[14] Mai, T.D., Mai, B.L., Pham, D.T., Nguyen, H.P., "Control of doubly-fed induction generators using Dspace R&D controller board – an application of rapid control coordinated with Matlab/Simulink", International Symposium on Electrical & Electronics Engineering, Track. 3, pp. 302-307, 2007.
[15] Hazzab, A., Commande des systèmes par logique floue, Réseau de neurones et Algorithmes géniques, Ph.D. thesis, University Mohamed Boudiaf USTO, Algeria, 2006.
[16] Hong, H.L., Phan, Q.D., Le M.P., Le D.K., Nguyen, H.N., "A few fuzzy logic approach for control system of wind turbine with doubly fed induction generator," IEEE International Forum on Strategic Technology (IFOST), pp.134-139, 2010.
[17] Porcyk, T. J. and Mamdani, E.H., "A linguistic self-organizing process controller," Automatic, vol.15, pp.15 – 30, 1979.
[18] Ram, A. G., Lincoln, A. S., "Fuzzy adaptive PI controller for single input single output non-linear system," ARPN, Journal of Engineering and Applied, Sciences. Vol. 7, NO. 10, pp. 1273-1280, 2012.
[19] Belabbes, A, Hamane, B., Bouhamida, M., Draou, A., Benghanem, M., "Power Control of a Wind Energy Conversion System based on a Doubly Fed Induction Generator using RST and Sliding Mode Controllers," International Conference on Renewable Energies and Power Quality (ICREPQ'12), Santiago de Compostella, Spain, 2012.
[20] Yao, X.I., Liu, Z.L, Cui G.S., "Decoupling Control of Doubly-Fed Induction Generator based on Fuzzy-PI Controller," IEEE 2nd International Conference on Mechanical and Electrical Technology (ICMET), pp. 226-230, Singapore, 2010.
[21] Hamane, B., Doumbia, M. L., Cheriti, A., Belmokhtar, K., "Comparative Analysis of PI and Fuzzy Logic Controllers for Matrix Converter," IEEE International Conference on Ecological Vehicles and Renewable Energies (EVER), pp. 1-7. Monte-Carlo (Monaco), 2014.
[22] Zakaria, K., Kamel, B, "Active and Reactive Power Control for Doubly-Fed Wound Rotor Induction Generator", IEEE, The fifth International Renewable Energy Congress (IREC14), pp.1 – 6, Hammamet, TUNISIA, 2014.
[23] Altun, H., Sünter, S., "Modeling, Simulation and Control of Wind Turbine Driven Doubly-Fed Induction Generator with Matrix Converter on the Rotor Side", Electrical Engineering, Vol.95, Issue 2, pp. 157-170, June 2013.
[24] Afonso, L. P., Pinto, S. F., Silva, J. F., "Maximum Power Point Tracker for Wind Energy Generation Systems using Matrix Converters", IEEE, 4th International Conference on Power Engineering, Energy and Electrical Drives (POWERENG13), pp.978-983, Istanbul, Turkey, 2013.
[25] Kenneth, E. O., Uhunmwangho, R., "Matrix Converter Control for DFIG", IEEE International Conference on Emerging & Sustainable Technologies for Power & ICT in a Developing Society (NIGERCON), pp. 273 – 277, Owerri, 2013.
[26] Suman. M., Debaprasad, K., "Improved Direct Torque and Reactive Power Controlof a Matrix Converter Fed Grid Connected DoublyFed Induction Generator,"IEEE Transactions on Industrial Electronics, Vol: 62, Issue: 12, pp.7590 – 7598, 2015.

Appendix

Table 3.DFIG Parameters

Parameters	Values
Rated line supply voltage V_s	398 / 690 V
Grid frequency f_s	50 Hz
Frequency switch f_{sw}	4000 Hz
Rotor rated voltage V_r	225 / 389 V
Rated frequency rotor f_r	14 Hz
Stator resistance R_s	0.012 Ω
Rotor resistance R_r	0.021 Ω
Pair of poles P	2
Statoric inductance L_s	0.0137 H
Rotor inductance L_r	0.0136 H

Mutual inductance L_m	0.0135 H
Friction coefficient f	0.0024 N. m. s^{-1}
Moment of inertia J	1000 kg. m^2
Filter capacitor C_f	0.075 F
Filter inductor L_f	400 mH

Parameters	Values
Blades radius R	35.25 m
Gain of gearboxε	90
Air density ρ	1.225 kg/m^3

Table 4. Wind Turbine Parameters